Supplemental Material for
"Topological protection can arise from thermal fluctuations and interactions"

Ricardo Pablo Pedro,[1,*] Jayson Paulose,[2,*] Anton Souslov,[3,4] Mildred Dresselhaus,[5] and Vincenzo Vitelli[3,†]

[1] *Department of Chemistry, Massachusetts Institute of Technology, Cambridge, MA 02139, USA*

[2] *Department of Physics and Institute of Theoretical Science, University of Oregon, Eugene, OR 97403, USA*

[3] *The James Franck Institute and Department of Physics, The University of Chicago, Chicago, IL 60637, USA*

[4] *Department of Physics, University of Bath, Bath BA2 7AY, United Kingdom*

[5] *Department of Physics and Department of Electrical Engineering and Computer Science, Massachusetts Institute of Technology, Cambridge, MA 02139, USA*

SIMULATION DETAILS

We performed 2D molecular dynamics simulations in which directed lines are approximated as discrete chains of N beads (monomers) of mass m connected by nonlinear springs with equilibrium length l_0 and maximum extension $l_{\max}$, implemented using the pair potential

$$V_{\text{chain}}(r) = -\frac{Kl_{\max}^2}{2}\log\left[1-(r-l_0)^2/l_{\max}^2\right] \tag{1}$$

for linked beads with separation r. To implement the noncrossing constraint, each bead has a finite radius $r_{\text{c}} = l_0$ and interacts with all other beads via a harmonic contact potential $V_{\text{c}}(r) = k_{\text{c}}(r-l_0)^2,\ r < l_0$. Tension is applied by pulling the topmost bead along the y direction with a force τ. The bottom beads are either pinned to specific points with horizontal spacing a at $y = 0$ (for simulations in Fig. 1) or confined to $y = 0$ but free to slide along the x direction (for Figs. 2 and 3). The substrate interaction $V(x, y)$ per unit length is implemented as a position-dependent potential of strength $l_0V(x, y)$ acting on every bead. For all simulations, we set $m = 1$, $l_0 = 0.3$, $K = k_{\text{c}} = 10^3$, $\tau = 10$, $a = 1$, $\lambda = 25$ in simulation units. The simulation box size is $L_x = 10a$ and $L_y = 16\lambda$ with periodic boundary conditions along x. The box size along y is always many times the chain length.

Temperature is implemented by applying a friction force with drag coefficient γ to all beads, and adding a random force of strength $\sqrt{2\gamma k_{\text{B}}T}$ along each dimension to each bead. In all our simulations, we set $k_{\text{B}}T = 1$ and $\gamma = 0.5$ in simulation units. Newton's equations are solved using the velocity-Verlet algorithm with time steps of length 0.001 in simulation units, which equates to $0.0316/\omega$ where $\omega = \sqrt{k_{\text{c}}/m}$ is the contact-force time scale.

Simulations are initialized with straight, tension-free chains arranged parallel to the y axis and with horizontal spacing a along x. Each simulation is run for H time steps where H is of the order of 10^7. To aid equilibration, simulations begin with an annealing phase in which the temperature is set to 2–3 times the desired temperature and reduced to the final temperature via a linear ramp in time for the first $H/2$ steps. Equilibrium quantities such as density profiles are measured from snapshots of the bead positions taken at every 1000 to 2000 time steps for the last quarter of the simulation.

Disorder is implemented by adding to the substrate potential a superposition of n_{d} products of sine functions with random amplitudes, wavelengths, and phases:

$$V_{\text{d}} = \sum_{i=1}^{n_{\text{d}}} \alpha_i \sin\left(\frac{2\pi r_i}{L_x}x + \phi_i\right)\sin\left(\frac{2\pi s_i}{L_y}y + \varphi_i\right), \tag{2}$$

where amplitude α_i is drawn from a normal distribution with zero mean and standard deviation $2\sigma_{\rm d}/\sqrt{n_{\rm d}}$, and random phases ϕ_i and φ_i are uniformly distributed in the interval $[0, 2\pi)$. The amplitudes are chosen so that the root-mean-square deviation of the potential $V_{\rm d}$ over the entire substrate matches the desired disorder strength $\sigma_{\rm d}$.

To satisfy the periodic boundary conditions, the random wavelengths are integral fractions of the simulation box sizes (L_x, L_y), with r_i and s_i drawn uniformly from integers in the intervals $5 \le r_i \le 20$ and $8 \le s_i \le 32$ respectively. In Fig. 3, we use $n_{\rm d} = 8$ and 16.

Table I shows values of the situation-specific simulation parameters that have not been defined above.

Simulation	N	H	V_1	V_2
Fig. 3, $\mathcal{C} = 1$	250	2×10^7	0.3333	0.2333
Fig. 3, $\mathcal{C} = -1$	250	4×10^7	2	0.8
Fig. 4, $\mathcal{C} = 1$	130	5×10^7	0.3333	0.2333
Fig. 4, $\mathcal{C} = -1$	160	8×10^7	2	0.8
SM Fig. 1(b)	200	2×10^8	0.0667	0
SM Fig. 1(c)	200	2×10^7	0.0667	0

TABLE I. Simulation parameters

COMPUTING THE SCATTERING INTENSITY PROFILE

From the numerically averaged distribution of monomer density, we compute the scattering instensity profile. This quantity is proportional to the static structure factor $S(\mathbf{k})$ for the wavevector $\mathbf{k}$. The characteristic features of the scattering profile are the nearest-neighbor density peaks situated along the direction separating the chains (i.e., the direction perpendicular to the average chain orientation). These peaks are signatures of orientiational order in the chain liquid, and can be compared to the peaks observed in X-ray scattering profiles for nematic or smectic liquid crystals. Numerically, we compute the scattering intensity by taking the Fourier transform of the density-density correlation function, i.e., we compute $\langle \rho(\mathbf{k})\rho(-\mathbf{k})\rangle$. We plot the results in Figs. 3b,f of the main text.

MAPPING DIRECTED LINE PROBABILITY DISTRIBUTIONS TO QUANTUM-MECHANICAL WAVEFUNCTIONS

The probability distribution $\Psi(x_1, y|x_0, 0)$ describing the statistical weight of a chain with ends fixed at $x(0) = x_0$ and $x(y) = x_1$ can be expressed in terms of path integrals as

$$\Psi(x_1, y|x_0, 0) = \int_{x(0)=x_0}^{x(y)=x_1} \mathcal{D}\{x(y)\} \exp(-\beta E[x(y)]), \tag{3}$$

where $\beta = 1/(k_B T)$ is the inverse thermal energy scale, and the line energy E is a functional of $x(y)$ of the form

$$E = \int dy \left[\frac{\tau}{2} \left(\frac{dx(y)}{dy} \right)^2 + V[x(y)] \right]. \tag{4}$$

Upon discretizing the path integral above, the Schrödinger-like equation governing the change in partition weights due to the addition of a small element of length is given by Eq. (2) in the main text.

The many-body version of main text Eq. (2) is obtained by replacing the Laplacian operator ∂_x^2 with $\sum_i \partial_{x_i}^2$ and the potential $V(x)$ with a sum over pairs $\sum_{i<j} V(x_i - x_j)$.

GROUND-STATE DOMINANCE AND THE DIRECTED-LINE MOTT INSULATOR

To further develop the line-quantum mapping, we formally express the solution to partition function evolution, Eq. [2],in terms of the eigenstates ψ_n and corresponding eigenvalues ε_n of H [1]:

$$\Psi(X_0, y|x_0, 0) = \langle X_0| \left(\sum_n |\psi_n\rangle \, e^{-\beta \varepsilon_n y} \, \langle \psi_n| \right) |x_0\rangle \, . \tag{5}$$

Here, the initial and final "wavefunctions" $|X_0\rangle$ and $|x_0\rangle$ are identified with the probability distributions of the chain position at the initial and final locations: $|X_0\rangle = \delta(x - X_0)$ in the position basis. Equation (5) highlights a crucial feature of the imaginary-time evolution: at long distances from the origin, all contributions to Ψ become exponentially small compared to the ground-state contribution. This situation, known as *ground state dominance*, simplifies the description of long directed lines at equilibrium, which is completely captured by the ground state.

As an example of ground-state dominance for a single chain, we consider the evolution in the probability density function of a single directed line, pinned at $(x_0, 0)$, in a periodic potential of the form $V(x) = V_1 \cos(2\pi x/a)$. The eigenstates of H are Bloch waves of the form $\psi_{nk}(x) = u_{nk}(x)e^{ikx}$,

with cell-periodic functions $u_{nk}(x) = u_{nk}(x+a)$ of the same periodicity as the potential, and the normalization $\int dx\, \psi^*_{nk}\psi_{n'k'} = (2\pi/a)\delta_{n,n'}\delta(k-k')$ for wavevectors belonging to the first Brillouin zone (BZ) $k, k' \in [-\pi/a, \pi/a)$. All real combinations of Bloch waves contribute to the probability evolution; the pinning condition corresponds to a delta-function probability distribution $\delta(x-x_0)$ represented as $\langle x|x_0\rangle$, which has a nonzero overlap with eigenfunctions across the Brillouin zone. As y increases, however, the partition sum is dominated by states close to the ground state (red region in Fig. 1a, which is the $k = 0$ eigenstate of the lowest band and therefore carries equal weight on all lattice sites. As a result, the chain density becomes more delocalized at larger y, as verified in simulations of a single chain experiencing a periodic potential (Fig. 1b).

As described in the main text, noncrossing interactions among lines can be exploited to prepare the directed-line system in the analogue of a Mott-insulating state at a density of one chain per lattice constant a. In the absence of any variation along the (imaginary) time axis, a signature of the Mott-insulating state is that lines are confined to their respective potential wells due to repulsion with their neighbours. In Fig. 1c–d, we verify this fact for the y-independent potential. Simulations of a system of noncrossing lines experiencing the same substrate potential as the single chain in Fig. 1b, at the density needed to "fill" the lowest band, show that the noncrossing condition confines each line to its respective well (Fig. 1c), even though the depth of the wells was not sufficient to confine a single line (Fig. 1b). The diffusive evolution of the probability distribution with length for the lone chain is overcome by line-line and line-substrate interactions under commensurate filling (Fig. 1d).

MANY-BODY POSITION OPERATOR FOR THE DIRECTED-LINE SYSTEM

The concept of adiabatic pumping is closely connected to the modern theory of electronic polarization [2, 3], which builds on the realization that changes in polarization and associated current flows in an electronic system undergoing an adiabatic change are not captured by the expectation value of the ordinary position operator x which is ill-defined under periodic boundary conditions. However, they are captured by an appropriately-defined many-body position operator [4, 5],

$$\langle X\rangle = \frac{L}{2\pi}\mathrm{Im}\ln\langle\Psi_0|\, e^{i\frac{2\pi}{L}\sum_{i=1}^{N} x_i}\,|\Psi_0\rangle\,, \tag{6}$$

where L is the system size.

Below, we apply this operator to the directed-line system. First, let us provide a quantitative description of the Mott-insulating ground state using Wannier functions associated with

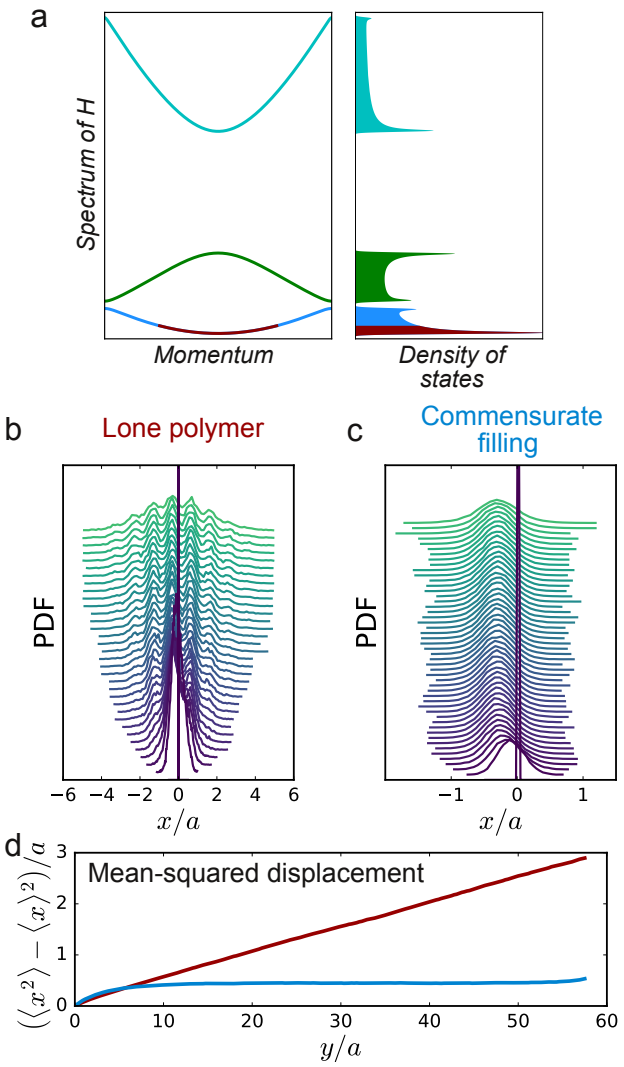

FIG. 1. **Mott insulator of noncrossing directed lines on a periodic substrate. a,** Example of the single-particle band structure for a potential with $V_2 = 0$ which is constant along y, and exhibits gaps in the spectrum. The probability distribution of a solitary chain is governed by states near the zero-momentum eigenstate of the lowest band (red area in **a**), and wanders over many lattice sites as shown by the spread of the probability density function of the chain position with distance from the pinning point (**b**). By contrast, under commensurate filling (having as many chains as potential periods along x), the ground state of the analogous fermionic system is a completely filled lowest band (blue and red areas in **a** combined), which puts the system in a Mott-insulating state with lines localized to individual potential valleys (**c**). **d,** The localization due to interactions in the many-line system (blue curve) tames the random-walk-like evolution of the position of a single chain (red curve) as evidenced by the mean square displacement of monomer position as a function of distance y (which equates to time in the diffusion problem).

the lowest band of the periodic potential. The Wannier functions, $W_{n,R}(x) = W_n(x - R)$ with

$W_n(x) = \frac{a}{2\pi}\int_{\mathrm{BZ}} dk\, \psi_{nk}(x)e^{-ikx}$, are a set of orthonormal basis functions for band n, each of which is associated with a unit cell at lattice vector $R = ja$ and exponentially localized around it. For fermions, Wannier functions are not uniquely defined because of a gauge freedom in defining the cell-periodic Bloch eigenstates $|u_{n,k}(y)\rangle$, but a real set of Wannier functions can always be found for isolated bands in one-dimensional periodic potentials [6]. When the number of chains equals the number of unit cells N, the fermionic ground state is obtained by assigning one line to each of the real Wannier functions spanning the lowest band $W_0(x - ja)$, $0 \leq j < N$, and computing a Slater determinant. The many-body ground state probability distribution of the directed-line system is then the absolute value of the fermionic ground state [7]: $\Psi_0^{\mathrm{P}} = |\Psi_0^{\mathrm{F}}|$, where Ψ_0^{P} and Ψ_0^{F} denote the directed-line and fermionic ground-state wavefunctions respectively. As a result, the mapping from fermions to bosons preserves expectation values of operators that commute with the position wavefunctions.

Continuous changes in the substrate potential shift the centres of mass of the Wannier functions. A striking result underlying the modern theory of electronic polarization is that these shifts can be expressed in terms of Berry phases of the cell-periodic Bloch eigenstates of the corresponding bands [2, 3, 8]. As a result, when the underlying lattice Hamiltonian $H(x + a) = H(a)$ undergoes a periodic change along the y axis $H(x, y) = H(x, y + \lambda)$, the shift in centre of mass $\langle x\rangle_n = \int dx\, xW_{n,0}^2(x)$ of the $R = 0$ Wannier function over one period is a topological invariant built upon the Berry phase, quantized by the Chern number $\mathcal{C}_n$. Note that the Chern number describes a shift in the centre of mass of the *real* Wannier functions which can be used to build the many-body states of the directed-line system.

Now we show that the position operator in Eq. (6) describes the flow of probability density of the chain positions under the imaginary-time Schrödinger evolution, Eq.[2].For comparison to the quantum case, we use t in place of y as the coordinate along the tension direction. We work with eigenstates $\psi_n(x, t)$ of the "Hamiltonian" $\beta H = -[(1/2\tau\beta)\nabla^2 - \beta V]$. For convenience we set $\beta = 1$ in the remainder of this section. The Hamiltonian is real, and hence has a set of real orthonormal eigenstates at each time (instantaneous eigenstates) with corresponding eigenvalues ε_n:

$$H(t)\psi_n(t) = \varepsilon_n(t)\psi_n(t), \tag{7}$$

and $\langle\psi_m(t)|\psi_n(t)\rangle = \int dx\psi_m(x, t)\psi_n(x, t) = \delta_{mn}$. We drop the spatial coordinate x in what follows. If we begin with the decomposition $\Psi(t_0) = \sum_n a_n(t_0)\psi_n(t_0)$, then we can always find the eigenfunctions at all times $\psi_n(t)$, and the solution $\psi(t)$ can always be written as as a superposition of these eigenfunctions, but the key to describing the evolution lies in finding the quantities $a_n(t)$.

We write the state at time t as

$$\Psi(t) = \sum_n a_n(t)\psi_n(t)e^{-\int_{t_0}^t \varepsilon_n(t')dt'}, \tag{8}$$

so that

$$\partial_t \Psi(t) = -H\Psi(t) \tag{9}$$

$$\Rightarrow \sum_n \left(-\varepsilon_n a_n\psi_n + \dot{a}_n\psi_n + a_n\dot{\psi}_n\right) e^{-\int_{t_0}^t \varepsilon_n(t')dt'} = -\sum_n \varepsilon_n a_n\psi_n e^{-\int_{t_0}^t \varepsilon_n(t')dt'} \tag{10}$$

$$\Rightarrow \sum_n \dot{a}_n\psi_n e^{-\int_{t_0}^t \varepsilon_n(t')dt'} = -\sum_n a_n\dot{\psi}_n e^{-\int_{t_0}^t \varepsilon_n(t')dt'}. \tag{11}$$

Using the orthogonality property, taking a dot product of the equation with ψ_m gives

$$\dot{a}_m = -a_m \langle\psi_m|\dot{\psi}_m\rangle - \sum_{n\neq m} a_n \langle\psi_m|\dot{\psi}_n\rangle e^{-\int_{t_0}^t (\varepsilon_n(t')-\varepsilon_m(t'))dt'}. \tag{12}$$

However, since we restrict ourselves to real orthogonal eigenstates, $\partial_t \langle\psi_m|\psi_m\rangle = 0 = \langle\dot{\psi}_m|\psi_m\rangle + \langle\psi_m|\dot{\psi}_m\rangle = 2\langle\psi_m|\dot{\psi}_m\rangle \Rightarrow \langle\psi_m|\dot{\psi}_m\rangle = 0$. (In quantum perturbation theory, this condition would be imposed by a "parallel transport" gauge choice $\langle\psi_m|\dot{\psi}_m\rangle = 0$). Hence,

$$\dot{a}_m = -\sum_{n\neq m} a_n \langle\psi_m|\dot{\psi}_n\rangle e^{-\int_{t_0}^t (\varepsilon_n(t')-\varepsilon_m(t'))dt'}. \tag{13}$$

If we begin in the ground state: $a_0(t_0) = 1$, then to lowest order we have $\dot{a}_0 = 0 \Rightarrow a_0(t) = 1$. However the coefficients of the excited states $m \neq 0$ have a lowest order contribution that is nonzero:

$$\dot{a}_m = -\langle\psi_m|\dot{\psi}_0\rangle e^{-\int_{t_0}^t (\varepsilon_0(t')-\varepsilon_m(t'))dt'}. \tag{14}$$

with initial condition $a_m(t_0) = 0$. In the adiabatic limit where variations happen over a time scale $T \to \infty$, we are satisfied with a solution to the above equations for $a_m(t)$ to lowest order in $1/T$. We obtain this by integrating once by parts to get

$$a_m(t) \approx \frac{\langle\psi_m|\dot{\psi}_0\rangle}{\varepsilon_0(t) - \varepsilon_m(t)} e^{-\int_{t_0}^t (\varepsilon_0(t')-\varepsilon_m(t'))dt'}. \tag{15}$$

The corrections to the above equations go as $\partial_t \langle\psi_m|\dot{\psi}_0\rangle \sim \langle\psi_m|\dot{\psi}_0\rangle /T$, and higher powers of $1/T$, as required for accuracy in the adiabatic limit. Finally, the time-evolved wavefunction at all times can be written using Eq. 8 as

$$\Psi(t) = e^{-\int_{t_0}^t \varepsilon_0(t')dt'} \left(\psi_0(t) + \sum_{m\neq 0} \frac{\langle\psi_m|\dot{\psi}_0\rangle}{\varepsilon_0(t) - \varepsilon_m(t)}\psi_m(t)\right). \tag{16}$$

At first glance, the time evolution of the ground state appears to depend on the lowest instantaneous eigenvalue. This is, however, an artifact: although the imaginary-time Schrödinger equation does not conserve probability, any computations involving the partition weight $\Psi(x,t)$ requires normalization by the partition sum $Z \equiv \int dx\, \Psi(x,t)$. Therefore, the overall magnitude of the time-evolved wavefunction is arbitrary and we may choose a factor that explicitly conserves net probability integrated over the span of the system:

$$\Psi(t) = \psi_0(t) + \sum_{m\neq 0} \frac{\langle \psi_m | \dot{\psi}_0 \rangle}{\varepsilon_0(t) - \varepsilon_m(t)} \psi_m(t), \tag{17}$$

for which $\langle \Psi | \Psi \rangle = 1 + O(1/T^2)$.

We are interested in the probability distribution of points in the interior of a directed line at $y = t$, far away from the ends at $y = 0$ and $y = L$, which is described purely by the ground state of the Hamiltonian regardless of pinning conditions. In addition to the partial partition weight $\Psi(x, t|x_0, 0)$ of finding the line at position x at y-coordinate t, we need to consider the weight $\Psi^\dagger(x, t|x_L, L)$ associated with conformations connecting the interior point at t to the pinning point at L. The complementary partition function is governed by the equation $-\partial_t \Psi^\dagger = [(1/2\tau\beta)\nabla^2 - \beta V]\Psi^\dagger = -\beta H \Psi^\dagger$. The dagger does not signify conjugation; Ψ and $\Psi^\dagger$ are different functions. However the notation is suggestive and the situation parallels that of a wavefunction and its conjugate in the quantum mechanical picture. Repeating the time-dependent perturbation theory calculation provides the following expression for $\Psi^\dagger(t)$:

$$\Psi^\dagger(t) = \psi_0(t) - \sum_{m\neq 0} \frac{\langle \psi_m | \dot{\psi}_0 \rangle}{\varepsilon_0(t) - \varepsilon_m(t)} \psi_m(t), \tag{18}$$

The spatial density distribution at y-coordinate t is written as:

$$\rho(x,t) = \frac{1}{Z} \Psi(x, t|x_0, 0) \Psi^\dagger(x, t|x_L, L), \tag{19}$$

where $Z = \int dx\, \Psi(x, r_0; t)\Psi^\dagger(x, r_1; t) = \Psi(x_L, L|x_0, 0)$ is the full partition function of the chain and therefore independent of t. We can treat Z as a time-independent normalization, and we will not write it explicitly in what follows. The time evolution of the spatial density produces a "probability current density" j through the continuity equation

$$\partial_t \rho(x,t) + \partial_x j(x,t) = 0 \tag{20}$$

$$\Rightarrow \partial_x j = -\Psi \partial_t \Psi^\dagger - \Psi^\dagger \partial_t \Psi \tag{21}$$

$$= \frac{1}{2\tau\beta} \left(\Psi \partial_x^2 \Psi^\dagger - \Psi^\dagger \partial_x^2 \Psi \right) - \beta V \left(\Psi \Psi^\dagger - \Psi^\dagger \Psi \right) \tag{22}$$

$$\Rightarrow j = \frac{1}{2\tau\beta} \left(\Psi \partial_x \Psi^\dagger - \Psi^\dagger \partial_x \Psi \right). \tag{23}$$

(we reintroduce the general β from now on).

The shift in expected position of the chain upon traversing a period T in "time" (i.e. distance along the chain) is now obtained by integrating the current density over a period and over all space. Substituting the perturbative expressions for Ψ and $\Psi^\dagger$ into the current equation, we get

$$j(x,t) = \frac{1}{2\tau\beta} \sum_{m\neq 0} \frac{\langle \psi_m | \dot{\psi}_0 \rangle}{\varepsilon_0(t) - \varepsilon_m(t)} \left[2\psi_m \partial_x \psi_0 - 2\psi_0 \partial_x \psi_m \right]. \tag{24}$$

Integrating over space to get the average current, we have

$$J(t) = \frac{1}{L} \int dx\, j(x,t) = \frac{2}{\tau\beta} \sum_{m\neq 0} \frac{\langle \partial_x \psi_0 | \psi_m \rangle \langle \psi_m | \partial_t \psi_0 \rangle}{\varepsilon_0 - \varepsilon_m}, \tag{25}$$

where we have used the orthogonality $\langle \psi_m | \psi_0 \rangle = 0$ which implies $\langle \psi_m | \partial_x \psi_0 \rangle + \langle \partial_x \psi_m | \psi_0 \rangle = 0$.

Using the fact that the instantaneous eigenstates ψ_i can always be chosen to be real for real Hamiltonians, the right hand side of Eq. 25 may be written as

$$J(t) = \frac{1}{\tau\beta} \sum_{m\neq 0} \left(\frac{\langle \partial_x \psi_0 | \psi_m \rangle \langle \psi_m | \partial_t \psi_0 \rangle}{\varepsilon_0 - \varepsilon_m} + \frac{\langle \partial_t \psi_0 | \psi_m \rangle \langle \psi_m | \partial_x \psi_0 \rangle}{\varepsilon_0 - \varepsilon_m} \right), \tag{26}$$

Upon identifying the quantum-mechanical momentum operator p with $-i\hbar\partial_x$ and substituting $\hbar^2/2m$ for $1/2\tau\beta$, the right hand side of Eq. 26 is identical to the average flow of current under adiabatic evolution of a quantum electronic system with the same potential $V(x)$ [4, 9, 10], which forms the basis for the theories of polarization and quantized charge pumping. Furthermore, for adiabatic evolution of the Hamiltonian, the current is the time-derivative of the expectation value of the many-body position operator:

$$J(t) = \frac{1}{L} \frac{d}{dt} \langle X \rangle. \tag{27}$$

Like the position operator, the probability flow therefore depends only on the square modulus of the instantaneous ground-state wavefunction [4]. Since the instantaneous adiabatic ground states of the directed line system are simply the absolute values of the corresponding ground states of the electron system and share the same form of their probability evolution over time, the equivalence of the two problems has been established.

The equivalence of the probability current with the quantum-mechanical system and the existence of exponentially localized Wannier functions for the directed line system also provides a route to rigorously proving the robustness of the tilt under many-body interactions and substrate disorder, following the techniques of Niu and Thouless [10].

CONFINEMENT IN EXPERIMENTAL REALIZATIONS

In our simulations, periodic boundary conditions with a fixed transverse width provide the most straightforward way to impose the density requirement of commensurate filling while allowing the chains to tilt. In experimental realizations, periodic boundary conditions are hard to implement, though not impossible (consider chains deposited on a cylindrical surface). However, setting up hard boundary conditions parallel to the x and y directions of the substrate potential would eventually cause chains to pile up at either wall due to their tilt. Here we discuss two possibilities for confinement of chains on a flat surface to maintain the correct density but allow chains to tilt without piling up at system boundaries.

For experimental realizations that require chains to traverse the system longitudinally without breaking (e.g. magnetic vortex lines) we envision confinement via an external harmonic trap in the transverse direction: a potential of the form $V(x, y) = (1/2)kx^2$ (constant in the longitudinal direction) which varies over length scales much larger than the lattice spacing. The strength of the harmonic potential could be tuned so that the chains attain the correct density (one chain per lattice spacing for filling the lowest band) over a broad region around the center of the trap. In this region, we would observe the quantized tilt in a finite "cloud" of chains. The absence of hard walls would mean that no pile-up arises, but the chains at the edges of the cloud would effectively be at lower density and would deviate from the perfect tilt. This would be a small perturbation if the high-density region has a sufficiently large number of chains. We note that similar confinement techniques have been used with success to measure the quantized charge pumping in clouds of cold atoms [11–13], which suffer from the same problem of confinement without hard walls. In those experiments, the quantized transport of the cloud of particles was shown to survive in the presence of the trap and edge effects.

A different approach, applicable to colloidosome- or polymer-based realizations which allow finite chain segments, would be to deposit a solution or melt of many chain segments, with lengths a few times the longitudinal wavelength λ, in a finite region (effectively, hard boundary conditions) with the box boundaries aligned with the x and y directions of the substrate potential. Commensurate filling could be achieved by tuning the total monomer density in the region. The fast decay of end effects provided by the excitation gap would mean that each segment attains a close-to-perfect tilt over most of its length. If the density is high enough, there would be few gaps among chains and the overall monomer density profile would be similar to that of the long continuous chains shown in Fig. 2b and 2f. In this situation, some pile-up of chains would occur at the hard boundaries in

this situation, but the effect of the hard walls would decay over distances of order of the typical segment length so that the interior of the region would again display a well-quantized tilt relative to the substrate potential and the external tension.

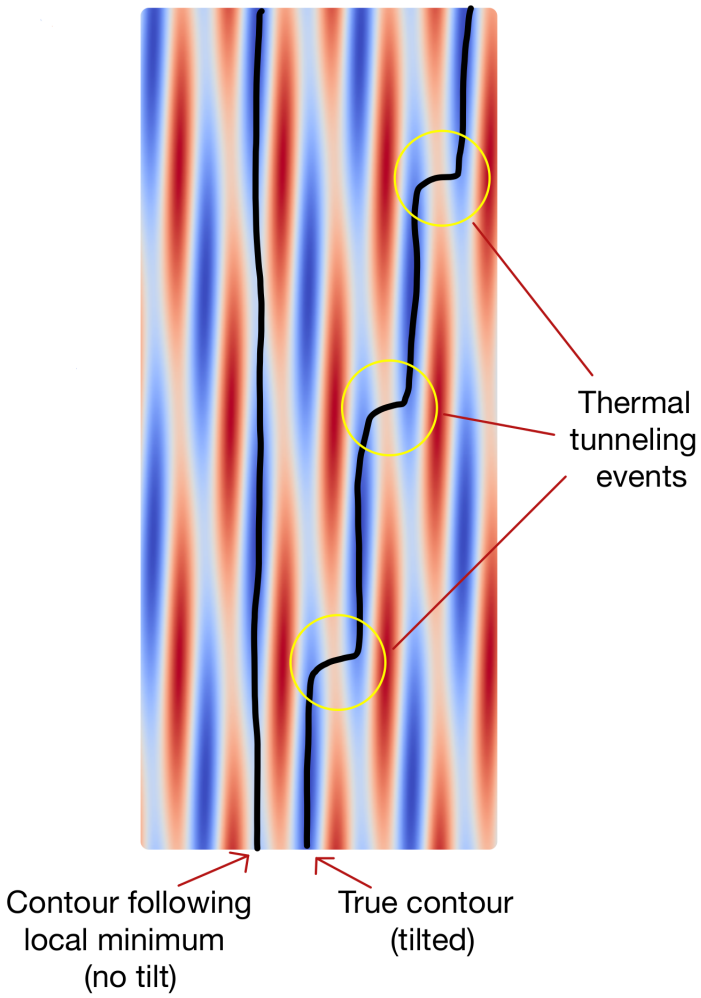

FIG. 2. **Thermal tunneling events are crucial for the topological tilt to arise.** The image schematically depicts the average contours of directed lines for the substrate with $C = 1$ in two scenarios. The contour on the left illustrates a directed line that follows the local minimum of the potential along its path, staying confined to a blue "valley" that it started out in at $y = 0$. As depicted, if the lines merely followed the local minimum, a tilted conformation would not arise. The contour on the right illustrates the mechanism leading to the tilted conformation observed in simulations: the directed line largely stays within potential valleys, but "tunnels" over a local maximum connecting two degenerate minima at specific values of y (highlighted). The tunneling events are analogous to the quantum-mechanical tunneling depicted for the electronic Thouless pump in Fig. 1 of the main text, but are a result of thermal (not quantum) fluctuations. The sketch highlights the nontrivial aspect of the Chern number calculation (it does not merely follow the shifts in local minima of the potential), as well as the crucial importance of thermal fluctuations in the topological tilt.

DESCRIPTIONS OF SUPPLEMENTAL MOVIES

The videos are the results of molecular dynamics simulations discussed in the 'Simulation details' section.

Movie 1

One chain fluctuating in a two-dimensional external potential. This chain does not exhibit a topologically protected tilt because there is no band gap to (diffusive) excitations. Instead, the chain diffuses freely over many lattice sites.

Movie 2

Nine chains fluctuating in a two-dimensional external potential with an incommensurate system size (corresponding to ten periods of the potential in the horizontal direction). In this video, the single vacancy (i.e., unfilled lattice site) diffuses freely much like the single chain in Movie 1. Despite strong interactions, there is no gap to excitations in this case of incommensurate lattice filling. Again, the chains do not exhibit a topologically protected tilt.

Movie 3

Ten chains fluctuating in a two-dimensional external potential with a *commensurate* system size, having exactly ten periods of the potential. Due to a gap in excitations, the individual chains no longer freely diffuse but are instead confined to their potential wells by strong repulsive interactions with their neighbors (c.f., SM Figure 1). In this case of commensurate filling the system does exhibit a topologically protected tilt.

---

* These authors contributed equally to this work.

† vitelli@uchicago.edu

[1] David R Nelson, "Defects and geometry in condensed matter physics," (Cambridge University Press, 2002) Chap. 9.

[2] R. D. King-Smith and David Vanderbilt, "Theory of polarization of crystalline solids," Physical Review B **47**, 1651–1654 (1993).

[3] Raffaele Resta, "Macroscopic polarization in crystalline dielectrics: the geometric phase approach," Reviews of Modern Physics **66**, 899–915 (1994).

[4] Raffaele Resta, "Quantum-Mechanical Position Operator in Extended Systems," Physical Review Letters **80**, 1800–1803 (1998).

[5] Raffaele Resta, "Manifestations of Berry's phase in molecules and condensed matter," Journal of Physics: Condensed Matter **12**, R107–R143 (2000).

[6] A. Bruno-Alfonso and D R Nacbar, "Wannier functions of isolated bands in one-dimensional crystals," Physical Review B **75**, 115428 (2007).

[7] M Girardeau, "Relationship between Systems of Impenetrable Bosons and Fermions in One Dimension," Journal of Mathematical Physics **1**, 516 (1960).

[8] J. Zak, "Berry's phase for energy bands in solids," Physical Review Letters **62**, 2747–2750 (1989).

[9] D. J. Thouless, "Quantization of particle transport," Physical Review B **27**, 6083–6087 (1983).

[10] Q Niu and D J Thouless, "Quantised adiabatic charge transport in the presence of substrate disorder and many-body interaction," Journal of Physics A: Mathematical and General **17**, 2453–2462 (1984).

[11] Shuta Nakajima, Takafumi Tomita, Shintaro Taie, Tomohiro Ichinose, Hideki Ozawa, Lei Wang, Matthias Troyer, and Yoshiro Takahashi, "Topological Thouless pumping of ultracold fermions," Nature Physics **12**, 296–300 (2016).

[12] Michael Lohse, Christian Schweizer, Oded Zilberberg, Monika Aidelsburger, and Immanuel Bloch, "A Thouless quantum pump with ultracold bosonic atoms in an optical superlattice," Nature Physics **12**, 350–354 (2015).

[13] Lei Wang, Matthias Troyer, and Xi Dai, "Topological Charge Pumping in a One-Dimensional Optical Lattice," Physical Review Letters **111**, 026802 (2013).